Spiral Meandering

Dwight Barkley
Mathematics Institute, University of Warwick, Coventry CV4 7AL, England

March 20, 1998

Abstract.
The complex, so called meandering, dynamics of spiral waves in excitable media is examined from the point of view of bifurcation theory. A computational bifurcation analysis is made of spiral dynamics. It is shown that spiral meandering is organized in parameter space around a codimension-two point where a Hopf bifurcation from rotating waves interacts with symmetries on the plane. A simple model of such a symmetric bifurcation then leads to a very simple picture for the wealth of spiral behavior.

Key words: Reaction-Diffusion, spiral waves, meandering

1 Introduction

Soon after the first observation of rotating spiral waves in what is now known as the Belousov-Zhabotinskii reaction [1, 2], Arthur Winfree noted in a footnote to a paper published in *Science* [3] that these spiral waves do not necessarily rotate rigidly about fixed centers. Winfree's careful examination revealed that the tips of spiral waves could trace out complex patterns as they rotate. He coined the term "meandering" for such non-periodic spiral dynamics. During the decade after this observation, neither experiments nor numerical simulations gave a clear answer to the question: "Do spiral waves in homogeneous, isotropic excitable media rotate periodically?". (The interested reader can find a brief history of the early work in this area on pages 181-183 of Ref. [4].) The issue is now resolved, both by high precision experiments [5, 6, 7, 8, 9, 10] and by fully resolved numerical studies [7, 11, 12, 13, 14, 15, 17]. The answer is simply that, depending on parameters of the system, spiral waves in excitable media can execute either periodic rotations or a fascinating variety of other deterministic dynamics. This chapter is a review of the current understanding of complexity of spiral dynamics from a bifurcation-theoretic view point.

Before delving into the details of bifurcation theory, I wish to elaborate more fully on the phenomena to be addressed. Figure 1 illustrates some of the variety of spiral states typically found in excitable media. These have been obtained from numerical simulations of a reaction-diffusion model discussed in the next section. Each state is represented by a segment of the path traced out by the spiral tip as it evolves in time. Figures 1(a) and (b) show periodic states; the spiral tips trace out circles as the waves rotate. (The definition of the spiral tip is given later in the chapter; it is not particularly important here.) Figures 1(c)-1(h) show a variety of meandering states; for these cases the tip paths are "flower" patterns of the type first observed by Winfree.

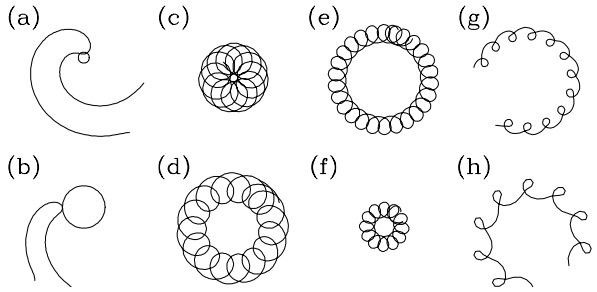

Fig. 1. Paths traced out by the tips of rotating spiral waves in a model excitable medium. For some values of the system control parameters, one finds periodic states as seen in (a) and (b). For these, spiral waves of constant shape rotate uniformly and the paths traced out by the spiral tips are circles. For other values of the control parameters, the spiral waves meander and the tip paths are "flower" patterns. Cases (c)-(h) show such tip paths after several (order 10) wave rotations. For these cases the spiral shape varies with time and the spirals are not shown. The figure is meant to illustrate *qualitatively* the variety of spiral states possible; the length scale is not the same for all paths shown. The model and parameter values are given in Secs. 2 and 3.3, respectively

If one looks at how spiral states in the model system are organized as a function of control parameters, one finds a dynamics landscape, or "flower garden" as shown in Fig. 2. In the nonlinear-dynamics literature, such a dynamics landscape is referred to either as a phase diagram or as a bifurcation set [18]. For the present discussion, the meaning of the two control parameters is not important. The relevant point is that the parameter plane is composed of three main regions separated by well define curves (bifurcation loci). There is a region in which spiral waves do not exist, a region in which spiral waves rotate periodically, and a region in which spiral waves meander. The meandering region can be further subdivided into a region in which flowers have inward-pointing petals and a region in which flowers have outward-pointing petals. Separating these two regions is a locus of meandering states whose petals lie along straight lines.

Figures 1 and 2 capture the essence of spiral dynamics in almost all homogeneous, isotropic two-dimensional excitable media. All the dynamics seen in these figures are intrinsic dynamics of isolated spiral waves. Even though the results shown have been obtained from a particular model system, all the states shown are observed in a variety of laboratory experiments [6, 7, 8, 9, 10] and numerical simulations [7, 11, 12, 13, 14, 15, 17]. Moreover, in every case in which a two-parameter survey has been conducted [10, 11, 15, 17], it has been found that spiral states are organized in parameter space qualitatively as shown in Fig. 2.

The aim of this chapter is to present the current understanding of the dynamics seen in Figs. 1 and 2 within the context of symmetric bifurcation theory. It will

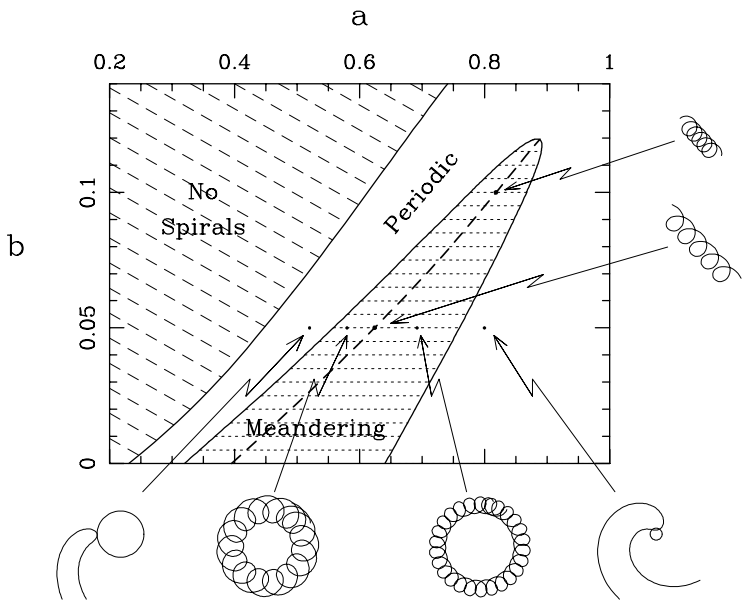

Fig. 2. Phase diagram or "flower garden" of spiral dynamics and a function of two control parameters in a reaction-diffusion model presented in Sec. 2. Diagrams such as this are now known to be common for spiral waves in excitable media. There are three main parameter regions containing: no spiral waves, periodically rotating spirals, and meandering spiral waves. Spiral tip paths illustrate states at 6 points. Small portions of spiral waves are shown for the two periodic cases. The paths for the meandering states are not closed curves. The meander region is itself separated into regions whose flowers have inward petals (left of dashed curve) and outward petals (right of dashed curve). On the dashed curve separating the two flower types, there are "infinite" flowers whose petals lie along straight lines. Two such states are shown. The diagram has been obtained with two of the four model parameters fixed: $\epsilon = 0.02$ and $D_v = 0$.

be shown, through a computational bifurcation analysis of reaction-diffusion equations, that the the dynamics landscape in Fig. 2 is organized around a parameter point at which a Hopf bifurcation interacts with symmetries of the plane. From this will follow a very simple description of the wealth of spiral behavior.

2 Reaction-diffusion model of excitable media

The model which my colleagues and I have used over the past several years in our studies of spiral waves is simple, two-variable reaction-diffusion model of the Fitzhugh-Nagumo type [13, 19]. It is a mathematical caricature of what is thought to take place in many real excitable systems. The model has the virtue of providing particularly fast time-dependent numerical simulations of spiral waves in continuous media. I will discuss this model with a view to providing the reader with a gen-

eral understanding of how excitability can arise in reaction-diffusion systems. The reader can find lengthy discussions of excitable media in Refs. [4, 20, 21, 22, 23].

Consider the general two-variable system of reaction-diffusion equations:

$$\begin{aligned} \frac{\partial u}{\partial t} &= f(u,v) + \nabla^2 u, \\ \\ \frac{\partial v}{\partial t} &= g(u,v) + D_v \nabla^2 v. \end{aligned} \tag{1}$$

where the variables u and v can be thought of as chemical concentrations in a hypothetical chemical reactions, or as membrane potential and current in a hypothetical physiological medium. The functions $f(u,v)$ and $g(u,v)$ model the local dynamics, e.g. chemical reaction kinetics, and the Laplacian terms account for diffusion in space. The length scale is chosen such that the diffusion coefficient for the u-variable is unity. D_v is thus the ratio of diffusion coefficients. The boundary conditions are taken to be no-flux, i.e. zero normal derivative, on the boundary of some domain of interest.

Two-variable models of the general form (1) are very common in the study of excitable systems [15, 20, 21, 22, 23], the Fitzhugh-Nagumo model being the most famous example. Various models differ principally in the choice of the reaction terms, i.e. the functions f and g. In addition, in many models the diffusion coefficient D_v is considered to be fixed, either with $D_v = 0$ (which is appropriate for modeling physiological media) or $D_v = 1$ (which is appropriate for modeling many chemical systems).

The reaction terms considered here are given by:

$$\begin{aligned} f(u,v) &= \frac{1}{\epsilon} u(1-u)\left[u - u_{\mathrm{th}}(v)\right], \\ \\ g(u,v) &= u - v, \end{aligned} \tag{2}$$

with,

$$u_{\mathrm{th}}(v) = \frac{(v+b)}{a},$$

where a, b, and ϵ are parameters, with $\epsilon \ll 1$. Due to the smallness of ϵ, the dynamics of the u-variable (referred to as the excitation variable) is typically much faster than the dynamics of the v-variable (referred to as the recovery variable).

To understand how excitability arises in this model, it is useful to consider the behavior of the system in the absence of diffusion, i.e. to consider the dynamics of the system:

$$\dot{u} = f(u,v), \quad \dot{v} = g(u,v). \tag{3}$$

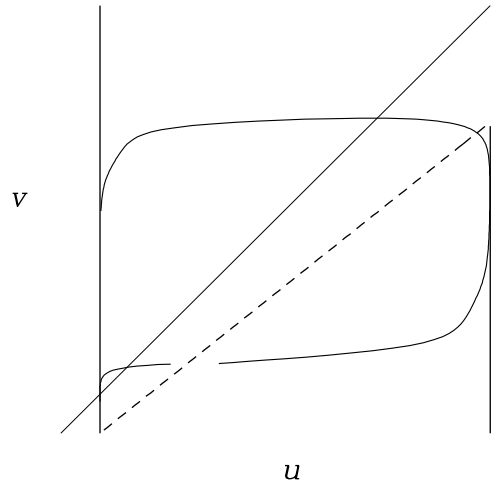

Fig. 3. Phase plane for the local dynamics of the model. The axes are the variables u and v. Shown are the system nullclines: the v-nullcline, $g(u,v) = 0$, is the line $v = u$, and the u-nullcline, $f(u,v) = 0$, has a backward "N" shape consisting of three lines: $u = 0, u = 1$, and $u = u_{\rm th}(v) = (v + b)/a$. An excitable fixed point sits at the origin where the u and v nullclines intersect. $u_{\rm th}$ is the excitability threshold for the fixed point. Schematic trajectories for two initial conditions are shown. The initial condition to the left of the threshold decays directly to the fixed point. The initial condition to the right of the threshold undergoes a large excursion before returning to the fixed point.

Figure 3 illustrates the phase-plane dynamics for Eqs. 3. Shown for reference are the nullclines defined by the curves $f(u,v) = 0$ and $g(u,v) = 0$. On these curves $\dot{u} = 0$ and $\dot{v} = 0$, respectively. The v-nullcline is a straight line and the u-nullcline has a backward "N" shape. The middle branch $u = u_{\rm th}$ has slope a and intercept $-b$. The system has a fixed point at the origin where the nullclines intersect (since there both $\dot{u} = 0$ and $\dot{v} = 0$). For $a > 0$ and $b > 0$ this fixed point is linearly stable, and hence all initial conditions sufficiently close to the fixed point decay directly to it.

The origin is nevertheless excitable. By this, one means that there exists a threshold such that initial conditions farther than the threshold from the fixed point do not evolve directly to it, but instead undergo a large excursion prior to reaching the fixed point. The threshold here is given by the middle branch of the u-nullcline: $u = u_{\rm th}(v)$. Initial conditions to the right of this threshold evolve quickly [due to the smallness of ϵ in Eqs. (2)] to the right branch of the u-nullcline, and hence initially move away from the fixed point. Eventually the trajectory brings the system back to the origin as shown. Thus all initial conditions evolve to the stable fixed point, but there is a dichotomy of behavior depending on whether the initial condition is to the right or left of the threshold.

The following terminology is used to describe the various possible states of the system. If the system is close to the fixed point, then it is said to be *quiescent*; if it is near the right branch of the u-nullcline, then it is said to be *excited*. If the system is near the left branch of the u-nullcline (i.e. $u \sim 0$) but v is not near zero, then the system is said to be *recovering*. Phase-space points in the recovering state are much further from the threshold than the points in the quiescent state.

The u-nullcline shown in Fig. 3 is not entirely correct because the three branches of $f(u, v) = 0$ actually extend past the corners of the backwards "N" where the $u = u_{\rm th}$ branch meets the branches $u = 0$ and $u = 1$. The corners in the u-nullclines are not found in other models of excitability and they are are somewhat problematic from the point of view of the local dynamics in this model. For spiral waves in a spatially extended medium, however, phase-space points never get close to the corners. The reason for having a u-nullcline with this particular shape is that it permits the equations to be simulated by a fast numerical scheme discussed momentarily.

Consider now the full reaction-diffusion system (1) describing a spatially extended medium. The combination of the local excitable dynamics illustrated in Fig. 3, and the diffusive coupling of nearby points in space is sufficient, in most cases, to permit waves of excitation to propagate in the extended system. The reason is as follows: if some spatial points in the medium are excited (i.e. near the right branch of the u-nullcline) while nearby points are quiescent, diffusion acts to "pull" the quiescent points the small distance in phase space needed to cross the threshold for excitation. Once across the threshold, the local kinetics take over and these points quickly become excited as well. In this way regions of excitation can spread through the extended medium. However, the local kinetics are such that excited points eventually return to the quiescent state. Thus no portion of the medium stays excited indefinitely and this allows the possibility of recurrent excitations, as occurs for example, with rotating spiral waves.

Most of what has been said until now applies equally to all two-variable models of the form given by Eqs. (1). The advantage of the model with the particular choice of reaction terms in Eqs. (2), is that this choice allows the model *to be simulated efficiently over a large range of spatio-temporal scales.* High-speed, coarse-grained simulations can be used to gain insight and explore parameter space at small computational expense, while high-resolution simulations can be used to assess the validity of low-resolution results. This is explained in detail in Ref. where a complete algorithm for time-stepping the equations is given.

The algorithm is based on the fact that the branches of the u-nullcline have a very simple form and it is possible to write a numerical scheme which time-steps the local u-dynamics implicitly. In the limit of timesteps large in comparison with

$1/\epsilon$, the algorithm for the local u-dynamics reduces to the following:

$$u^{n+1} = \begin{cases} 0 & \text{if } u^n < u_{\text{th}} \\ u_{\text{th}} & \text{if } u^n = u_{\text{th}} \\ 1 & \text{if } u^n > u_{\text{th}} \end{cases}$$

where u^n and u^{n+1} are the values of u at timesteps n and $n+1$, respectively. Thus in the limit of large timesteps (or equivalently the limit of small ϵ for fixed time step), u takes on just two values: 0 and 1. Hence the model gives rise naturally to cellular-automaton-type scheme for the fast dynamics. However, unlike cellular-automaton models of excitable media [24, 25, 26, 27], the model given by Eqs. (1) and (2) is a partial-differential equation and hence continuous in space and time. Moreover, it can be investigated by means other than time stepping, as I now discuss.

3 Bifurcation approach

Without a bifurcation analysis, it is nearly impossible to obtain a comprehensive understanding of any complicated nonlinear system and excitable media are no exception. While time-dependent simulations can tell us much about the behavior of a reaction-diffusion model, to understand fully the spiral dynamics illustrated in Figs. 1 and 2, one must attack the problem with additional, more efficient, methods. In this section I outline the bifurcation methods used to investigate spiral waves. Without going fully into the numerical details, I shall explain how one computes periodic spirals as steady states and how one computes the stability of these spirals by finding the leading eigenvalues and eigenvectors of the associated stability problem. Time-dependent simulations are necessary for studying the meandering states which bifurcate from periodic solutions and I shall provide further details concerning these simulations. The reader can find a general discussion of numerical bifurcation methods in Refs. [28, 29] and details of the solutions of large sparse systems in Refs. [30, 31, 32, 33, 34].

3.1 Steady states

Consider a periodically rotating spiral wave. Such a wave rotates as a rigid body and is seen as a *steady state* when viewed in a reference frame rotating at the angular frequency of the spiral. Figure 4 shows such a state. One can obtain a steady state equation for such periodic spiral waves by making a change of coordinates in Eqs. (1) to a system rotating at the spiral frequency ω_1, and demanding that the time derivatives in the rotating frame be zero:

$$0 = \frac{\partial u}{\partial t'} = f(u,v) + \omega_1 \frac{\partial u}{\partial \theta'} + \nabla'^2 u,$$
$$0 = \frac{\partial v}{\partial t'} = g(u,v) + \omega_1 \frac{\partial v}{\partial \theta'} + D_v \nabla'^2 v.$$

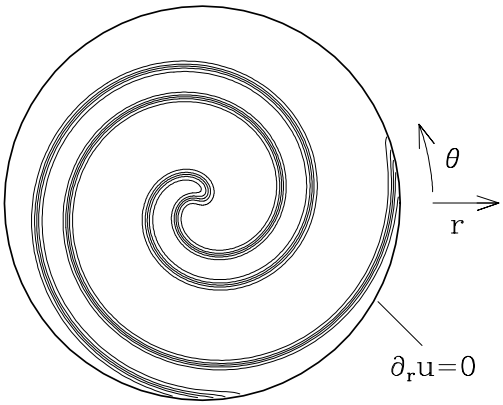

Fig. 4. Periodically rotating spiral wave computed via Newton's method. In the "laboratory" frame the wave rotates clockwise at constant speed and in a frame rotating with the angular frequency of the spiral it is a steady state. Due to rotational symmetry, the angular orientation of the spiral is arbitrary. Contours of the fast variable, u (equally spaced from $u = 0.1$ to $u = 0.9$), show the sharp transitions between the two branches, $u = 0$ and $u = 1$ of the u-nullcline. Contours of v are not shown. The model parameters are: $a = 0.643$, $b = 0.001$, $\epsilon = 0.02$, and $D_v = 0$; the domain has radius $R = 18$.

where primes indicate the rotating coordinate system. These equations can be written compactly as:

$$0 = \mathbf{F}(\mathbf{u}, \omega_1), \tag{4}$$

where

$$\mathbf{F}(\mathbf{u}, \omega_1) \equiv \mathbf{D}\nabla'^2\mathbf{u} + \omega_1 \partial_{\theta'}\mathbf{u} + \mathbf{f}(\mathbf{u}), \tag{5}$$

with $\mathbf{u} = (u, v)^T$, $\mathbf{D} = \mathrm{diag}(1, D_v)$, and $\mathbf{f}(\mathbf{u}) = (f(u, v), g(u, v))^T$. The boundary conditions on the operators are taken to be $\partial_r \mathbf{u} = 0$ on a circle of radius R.

Technically, Eq. (4) is a nonlinear eigenvalue problem, because in addition to determining the fields u and v, it determines the rotational frequency (nonlinear eigenvalue) ω_1. This is consistent with the fact that, due to rotational symmetry, solutions of (4) are determined only up to an arbitrary orientation in angle. One can eliminate the phase freedom in Eq. (4) by augmenting this equation with an additional constraint which pins the phase of the spiral. For example, demanding that $u = 1/2$ at some point will generally suffice. This extra constraint allows ω_1 to be treated as an additional unknown, thereby permitting the pair $(\mathbf{u}, \omega_1)$ to be computed in concert [28].

Equation (4) is solved numerically by representing all fields on a polar grid and solving the resulting discretized system by Newton's method. The only difficulty with this approach is that Newton's method requires solving large (albeit sparse) systems of linear equations. There are, however, good numerical methods for solving such systems; the method used goes by the acronym GMRES [30, 34].

The resolution which has been used in the computations reported here is $N_r = 121$ radial and $N_\theta = 256$ azimuthal grid points. The u-field is fully resolved. All operators are evaluated spectrally in the θ-direction and using fourth-order finite differences in the r-direction (except at $r = R$ where second-order is used). Newton iterations are stopped when $||\mathbf{F}(\mathbf{u}, \omega_1)|| < 10^{-2}$; which is more than 100 times smaller than can reasonably be obtained by time-stepping Eqs. (1). The norm refers to the L_2 norm of the $2 \times N_r \times N_\theta$ discrete field values. Newton iterations are started from a solution obtained by direct simulation of Eqs. (1). Continuation can then be used to obtain rotating-wave solutions at other parameter values, including parameters at which these solutions are unstable.

3.2 Stability

After obtaining rotating wave solutions, the next step of a bifurcation analysis consists of determining the stability of the solutions by finding the leading eigenvalues (those with largest real part) and eigenvectors of the associated linear stability problem:

$$\mathbf{A}(\mathbf{u}, \omega_1) \cdot \tilde{\mathbf{u}} = \lambda \, \tilde{\mathbf{u}} \tag{6}$$

where λ and $\tilde{\mathbf{u}}$ are the eigenvalues and eigenmodes of the operator $\mathbf{A}(\mathbf{u}, \omega_1)$ defined by:

$$\mathbf{A}(\mathbf{u}, \omega_1) \equiv \mathbf{D}\nabla'^2 + \omega_1 \partial_{\theta'} + \mathbf{df}(\mathbf{u}). \tag{7}$$

The operator $\mathbf{A}(\mathbf{u}, \omega_1)$ is the linearization, i.e. Jacobian, of $\mathbf{F}(\mathbf{u}, \omega_1)$ in Eq. (4) about the steady-state (rotating-wave) solution $\mathbf{u}$.

The leading eigenvalues of $\mathbf{A}(\mathbf{u}, \omega_1)$ determine the stability of a periodic spiral wave: if none of the eigenvalues, λ, of $\mathbf{A}(\mathbf{u}, \omega_1)$ have positive real part, then the wave is stable. If at least one eigenvalue of $\mathbf{A}(\mathbf{u}, \omega_1)$ has positive real part, then the wave is unstable. Of particular interest will be bifurcations, signaled by the crossing of eigenvalues from the left to the right half of the complex plane. Also of importance are eigenvalue and eigenmodes associated with symmetries. These are discussed in Sec. 4.3.

The leading eigenvalues and corresponding eigenmodes in Eq. (6) are obtained by direct application of the methods in Ref. [31]. This is essentially the power method. The same polar grid used for the steady state computations is used for solving the eigenvalue problem. For the results reported, the five leading eigenvalues have been obtained to within the accuracy: $||\mathbf{A}(\mathbf{u}, \omega_1) \cdot \tilde{\mathbf{u}} - \lambda \, \tilde{\mathbf{u}}|| < 10^{-4}$.

3.3 Simulations

Meandering states cannot presently be computed by solving a fixed-point problem; for these it is necessary to resort to direct time-dependent simulations of the reaction-diffusion equations (1). A uniform square grid is used with no-flux boundary conditions imposed on the sides of a square domain. For all simulations reported, the domains are sufficiently large that the 4-fold symmetry of the domain boundary is entirely irrelevant, and the spiral dynamics are indistinguishable

from those in a rotationally symmetric system. The size of the domain used in simulations varies depending on the size of the flower pattern generated by the meandering spiral wave. For the infinite flowers shown in Fig. 2 (those whose petals lie along straight lines), no computational domain is large enough to contain the spiral tip indefinitely. For these cases, simulations are done in a box large enough to allow the spiral waves to travel significant distances before reaching the edge of the domain.

All the simulations reported in this chapter are fully resolved. A first-order Euler method is used for time-stepping the equations. The Laplacian terms in the reaction-diffusion equations are approximated with a 9-point finite-difference formula, which to leading order, eliminates the underlying 4-fold symmetry of square grid [13]. (For spiral waves in excitable media, anisotropies in the grid have a far greater effect on solutions than do anisotropies in the boundaries.)

For reference, the grid spacing for most results is $h = 0.1$ with a time step of $\triangle t = h^2/5$. The parameter values for the states shown in Fig. 1 are: (a) $a = 0.80$, $\epsilon = 0.02$, (b) $a = 0.52$, $\epsilon = 0.02$, (c) $a = 0.57$, $\epsilon = 0.02$, (d) $a = 0.58$, $\epsilon = 0.02$, (e) $a = 0.39$, $\epsilon = 0.01$, (f) $a = 0.42$, $\epsilon = 0.01$, (g) $a = 0.692$, $\epsilon = 0.02$, and (h) $a = 0.72$, $\epsilon = 0.02$, with $b = 0.05$ and $D_v = 0$ throughout.

4 Spiralogy

I return now to the spiral flower garden presented at the outset. After providing some needed kinematical preliminaries, I will report the results of a bifurcation analysis of these spiral dynamics.

4.1 Kinematical preliminaries

Figure 5 shows a sequence of spiral states obtained as a function of the parameter a in the reaction-diffusion equations (1) and (2) with the parameters b, ϵ, and D_v fixed: $b = 0.05$, $\epsilon = 0.02$ and $D_v = 0$. This sequence of states corresponds to a horizontal cut through the phase diagram in Fig. 2 at $b = 0.05$. Figure 6 shows, in more detail, states along this parameter cut near the transition between periodic and meandering spirals at "large" a.

Each state in Fig. 5 is represented, as before, by a plot of the path traced by the spiral tip over several (order 10) wave rotations. The spiral tip is here defined to be the point in space where $f(u = 1/2, v) = 0$, i.e. the point where $f = 0$ on the $u = 1/2$ contour of the spiral solution. This tip definition has been chosen because it can be computed easily and accurately from solutions fields. For the purposes here the tip location is simply a convenient projection of the instantaneous state of the system onto the two-dimensional plane.

4.1.1 Rotating waves

The periodically rotating spiral waves are examples of a more general class of dynamical states known as rotating waves (RW). These are, by definition, uniformly-

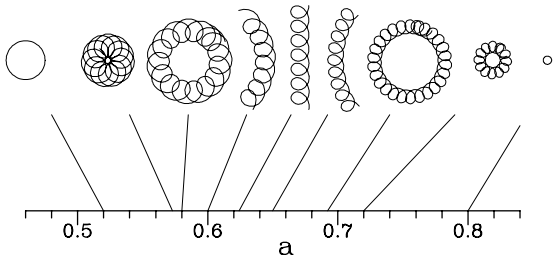

Fig. 5. Spiral states in the reaction-diffusion model as a function of the control parameter a with the other parameters fixed: $b = 0.05$, $\epsilon = 0.02$, and $D_v = 0$. This diagram corresponds to a one-parameter cut through the phase diagram in Fig. 2. As before, states are represented by tip-path plots. The length scale is the same for all plots. Several of the states shown also appear in Figs. 1 and 2.

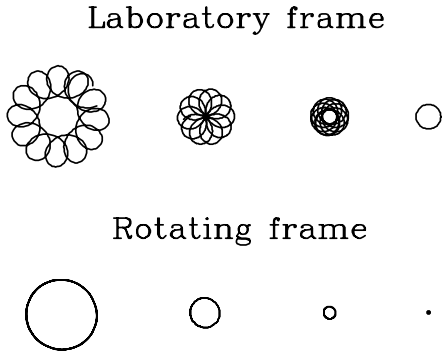

Fig. 6. Tip-path plots for rotating wave (RW) and modulated rotating wave (MRW) states in both the laboratory frame and in the rotating frame. The MRW states are quasiperiodic in the laboratory frame and periodic in the rotating frame. The rotating wave is periodic in the laboratory frame and steady in the rotating frame. The parameter values are the same as in Fig. 5 with (from left to right): $a = 0.72$, $a = 0.755$, $a = 0.746$, and $a = 0.80$.

rotating periodic states occurring in rotationally symmetric systems [13, 35, 36, 38]. Figure 6 shows the tip path of a RW state both in what I shall call the "laboratory" reference frame [the frame of reference of reaction-diffusion equations (1)], and the rotating reference frame (the frame of reference rotating at the spiral frequency ω_1). In the laboratory frame, the tip path is a circle whose radius will be denoted r_1. When view in the rotating frame, RW solutions are steady states and the tip path is therefore a fixed point. The RW solutions are actually computed in the

rotating frame, as described in Sec. 3.1.

4.1.2 Modulated rotating waves

The meandering states shown in Figs. 5 and 6 (except for the "infinite" flower at $a = 0.624$ in Fig. 5), are examples of a general class of dynamical states known as modulated rotating waves (MRW). These occur in rotationally symmetric systems and are two-frequency quasiperiodic states which are *periodic* when viewed in an appropriately rotating reference frame [13, 36, 38]. Fig. 6 shows three MRW states in the laboratory and rotating reference frames. In the laboratory frame the MRW states are quasiperiodic; the tip paths are not generically close orbits and after many wave rotations the tip paths fill out an annular region. In the rotating frame, the tip paths are closed periodic orbits. These closed orbits are close to, but not exactly, circular [13].

A convenient measure of the amplitude of the MRW states is the amplitude of the secondary motion of the spiral tip. Specifically, let r_2 be defined as the "radius" of tip orbit in the rotating frame, with the convention that r_2 be positive for states outward petals and negative for states with inward petals. Because tip orbits in the rotating frame are not truly circular, "radius" here means 1/2 the maximum distance between any pair of points on the tip orbit in the rotating frame.

The primary rotational frequency, ω_1, for a MRW state is defined to be the rotational frequency of the reference frame that renders the state periodic. This definition is the natural extension of the definition used for RW solutions. With this definition, ω_1 varies continuously in going from the RW to the MRW states. The secondary frequency is defined as: $\omega_2 \equiv 2\pi/\tau$, where τ is the period of the orbit in the rotating frame. That is, ω_2 is the frequency seen in the rotating frame of reference. The MRW states with outward petals are such that $\omega_2 > \omega_1$, whereas the states with inward petals are such that $\omega_2 < \omega_1$. This will prove significant in what follows.

4.1.3 Modulated traveling waves

The "infinite" flower in Fig. 5 that separates the MRW states with inward and outward petals is an example from a class of states known as modulated traveling waves (MTW). These are states which are periodic in a uniformly *translating* reference frame. Strictly speaking, they occur only in spatially infinite or spatially periodic systems [38]. However, these states behave indistinguishably from those which would be found in infinite medium, so long a the spiral center is far from any boundary. The MTW solutions can travel in any direction; the direction being determined by initial conditions.

4.2 Analysis in one parameter

With these definitions at hand, I turn to the quantitative analysis of spiral dynamics in the reaction-diffusion model, starting with the dynamics as a function of the parameter a, the other parameters being fixed as in the one-parameter cut

shown in Figs. 5 and 6: $b = 0.05$, $\epsilon = 0.02$ and $D_v = 0$.

Consider first the RW solutions as a function of a. In Fig. 5 stable RW states are seen both at "low" and "high" values of a. These states are, in fact, on a single branch of solutions which is unstable at intermediate values of a, (where the stable modulated waves are observed). This branch of RW solutions, together with its stability, has been computed as described in Secs. 3.1 and 3.2. The results are shown in Fig. 7.

Figure 7(a) shows three states on the RW branch. The states at the two ends are the same two stable solutions shown in Figs. 1, 2, and 5. The middle solution lies on the unstable portion of the RW branch.

Figures 7(b) and 7(c) show the behavior of eigenvalues along the RW branch. There is a complex conjugate pair of eigenvalues which, as the parameter a is increased, first cross the imaginary axis transversely into the right half plane and then cross transversely back into the left half plane. Hence, the stability limits of the RW branch are marked by a pair of *Hopf bifurcations*. Such Hopf bifurcations from rotating-wave solutions are sometimes called *secondary* Hopf bifurcations, but I shall not use this terminology. Note that not only are the RW states at "low" and "high" on a single branch of solutions, but also there is a single complex pair of eigenvalues responsible for the Hopf bifurcations at both end of the branch.

These Hopf bifurcations from the RW solutions introduce a second frequency into the spiral dynamics and give rise to the quasiperiodic MRW solutions. Figure 8 shows the bifurcation diagram for MRW states. The (dimensionless) radius ratio r_2/r_1 is plotted as a function of the bifurcation parameter a. Also indicated with a horizontal line are the RW states (for which $r_2 = 0$). The line is dashed between the Hopf points to indicate unstable RW states.

The MRW states are stable, and in the vicinity of the Hopf bifurcation points, the radius ratio grows as the square root of the distance from the bifurcations. Hence, the Hopf bifurcations are supercritical. Figure 6 shows several states near the upper-a Hopf bifurcation, both in the laboratory and rotating reference frames.

Away from the Hopf bifurcations, the radius ratio ceases to obeys the square-root scaling and the secondary radius diverges as the value of a approaches that where the MTW (modulated traveling wave) state is found. It is too expensive computationally to simulate states with very large radius ratio, and so there is a gap in the bifurcation diagram over the range of a where $|r_2/r_1| > 10$.

The following characterizes the frequency behavior (not shown) for the MRW states. Both ω_1 and ω_2 vary continuously with the parameter a. There is no entrainment (frequency locking) between the two frequencies of MRW states, that is, there are no parameter intervals (steps) over which the frequency ratio is a constant rational number. This is a general feature of MRW solutions first proved by Rand [36].

Finally, at the Hopf bifurcation points, the secondary frequency, ω_2, equals the imaginary part of the bifurcating eigenvalue, and the primary frequency, ω_1, equals the rotational frequency (also called ω_1) of the bifurcating RW state. The MRW

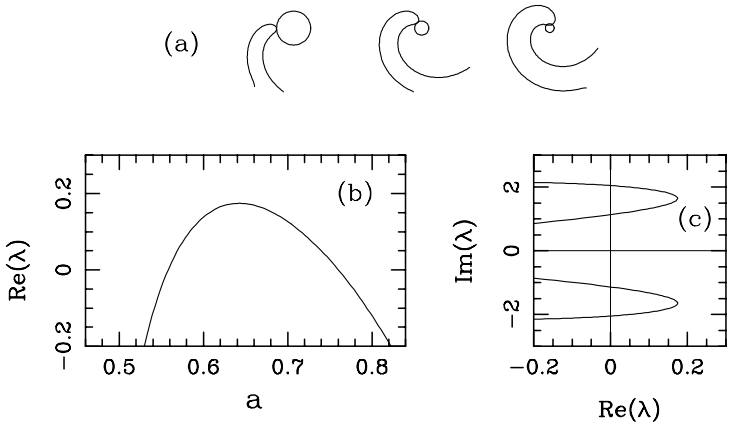

Fig. 7. Stability results for the branch of rotating wave solutions along the one-parameter cut shown in Fig. 5. (a) three states on the RW branch; the end two are the stable states seen in Fig. 5, and the middle is an unstable state. The values of a are (from left to right): $a = 0.52$, $a = 0.62$, and $a = 0.80$. In addition to the tip paths, the $u = 1/2$ contours of the u-field are shown near the spiral tip. (b) Real part of the bifurcating eigenvalues along the RW branch. Positive values correspond to unstable spiral states. (c) Bifurcating eigenvalues in the complex plane; arrows indicate the direction of increasing a. A complex pair of eigenvalues crosses the imaginary axis into the right half plane and then back into the left half plane. Both crossings are transverse and correspond to Hopf bifurcations.

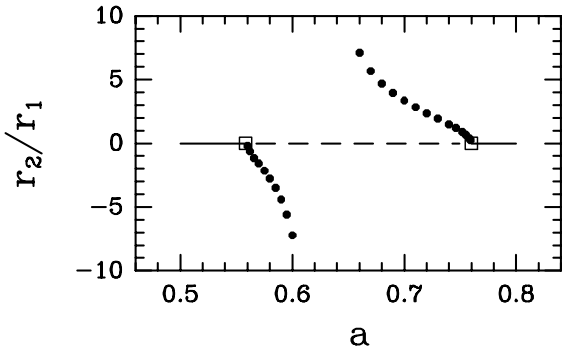

Fig. 8. Bifurcation diagram for the one-parameter cut shown in Fig. 5. The radius ratio, r_2/r_1, for MRW states is plotted as a function of the parameter a. Also shown, as a horizontal line, is the branch of RW states (for which $r_2 = 0$); solid indicates stable RW states and dashed indicates unstable RW states. The hollow squares denote Hopf bifurcation points. Both Hopf bifurcations are supercritical and near the bifurcations the radius ratio scales as the square-root of the distance from the bifurcation points. The radius ratio diverges as a approaches the value where exists a modulated traveling wave state.

states which bifurcate at "low" a have inward petals and satisfy $\omega_2/\omega_1 < 1$, whereas the states with outward petals which bifurcate at "high" a satisfy: $\omega_2/\omega_1 > 1$. The frequency ratio goes to 1, as a approaches the point where the MTW state is found.

4.3 The organizing center

Consider once again the two-parameter phase diagram in Fig. 2. In the preceding section the dynamics along a particular one-parameter cut through this diagram was considered in some detail. There are many other one-parameter paths which would yield, qualitatively, the same dynamics. In particular, all cuts at constant b, that pass through the region of meandering spirals, are essentially equivalent.

Near the apex of the meander region, however, where the locus of modulated traveling waves ("infinite flowers") meets the meander boundary, all the flower states observed along one-parameter cuts coalesce. This point is the *organizing center* for the phase diagram in Fig. 2: arbitrarily close to this codimension-two point there are stable rotating waves, modulated rotating waves with flowers of both types, and modulated traveling waves. This point is thus the key to understanding the variety of spiral behavior. In this section a bifurcation analysis of RW solutions is used to investigate the nature of the organizing center.

It is clear from the preceding section that the boundary of the meander region is simply a locus of Hopf bifurcations from RW states. In fact, the meander boundary plotted in Fig. 2 has been obtained by computing the locus of such Hopf bifurcations. Hence, all along the meander boundary the RW states have a complex-conjugate pair of eigenvalues on the imaginary axis. These eigenvalues, associated with Hopf bifurcations, are shown as squares in Fig. 9. The eigenvalues are denoted $\pm i\omega_2$, because the imaginary part of the bifurcating eigenvalues are equal to the secondary frequencies at the bifurcations (Sec. 4.2). These eigenvalues are on the imaginary axis only at the Hopf bifurcations; generically they cross the axis transversely as a function of the parameters a and b.

As can be seen in Fig. 9, there are eigenvalues (indicated with crosses) on the imaginary axis other than just those associated with the Hopf bifurcations. These eigenvalues result from symmetries of the system and are always on the imaginary axis. To understand the codimension-two point, one must understand these eigenvalues.

Consider first the eigenvalues at zero in Fig. 9. These eigenvalues are associated with rotational symmetry: because any rotation of a RW state is also a RW state, these states must always have a zero eigenvalue. The corresponding eigenmode is given by: $\tilde{u}_R = \partial_\theta u$, where $\tilde{u}_R$ is the eigenmode, u is the RW state, and θ is the polar angle. It can be verified by direct substitution into Eq. (6) that this is an eigenmode with zero eigenvalue.

The complex symmetry eigenvalues seen in Fig. 9 are associated with translational symmetry. While the computational domain used to compute the RW solutions is not translationally invariant, the computations find eigenvalues and eigenmodes which are virtually indistinguishable from those resulting from trans-

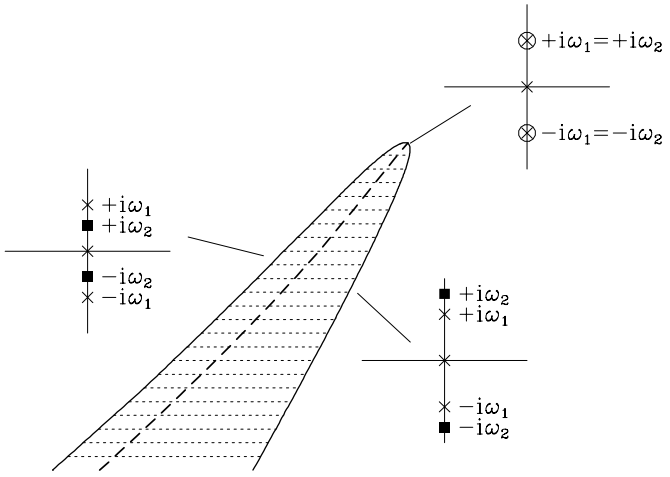

Fig. 9. Eigenvalues along the Hopf locus forming the boundary of the meander region. *Schematic* eigenvalue spectra are shown at three points on the Hopf locus. Squares denote Hopf eigenvalues and crosses denote symmetry eigenvalues. The spectra on the right and left branches of the Hopf locus differ, qualitatively, only in the ordering of eigenvalues on the imaginary axis. At the codimension-two point $\omega_1 = \omega_2$, and the stability operator has eigenvalues $\pm i\omega_1$ each with multiplicity two, plus a zero eigenvalue. This point is the organizing center for spiral dynamics. Note that the locus of modulated traveling waves emanates from this point.

lational symmetry. It can be verified [16] by direct substitution into the eigenvalue equation (6), that in an infinite, homogeneous system, a spiral rotating at frequency ω_1 has translational eigenmodes of the form $\tilde{u}_T = \partial_x u \pm i\partial_y u$, with eigenvalues $\lambda_T = \pm i\omega_1$. The eigenvalues obtained numerically are indistinguishable from $\pm i\omega_1$. In particular, extrapolation from domains with small radii shows that at radius $R = 18$ (as in Fig. 4), $|Re(\lambda_T)| < 10^{-45}$. Hence, these eigenvalues can be considered to lie on the imaginary axis.

Everywhere on the Hopf locus in Fig. 9, except at the codimension-two point, the five eigenvalues on the imaginary axis are distinct. Apart from the ordering of eigenvalues, there are no qualitative differences between the spectra on the right branch, $\omega_1 < \omega_2$, and left branch, $\omega_1 > \omega_2$, of the Hopf locus.

At the codimension-two point $\omega_1 = \omega_2$, and there is a resonance between the primary and secondary frequencies of the spiral wave. This is consistent with the fact that the locus of modulated traveling waves (for which $\omega_1 = \omega_2$), emanates from this point on the Hopf locus. At the codimension-two point, the Hopf and translational eigenmodes of the RW states coincide and the stability operator has eigenvalues $\pm i\omega_1$ each with multiplicity two, plus a zero eigenvalue. This specifies completely the codimension-two bifurcation to linear order.

To gain a deeper understanding of the organizing center, one needs to under-

stand the codimension-two bifurcation to higher order. For this one turns to a weakly non-linear analysis, which is the subject of the next section.

5 Towards a normal form for spiral dynamics

Given the evidence in the preceding section that the meandering dynamics of spiral waves are organized around a particular codimension-two bifurcation, one would hope that bifurcation theory could be applied to the problem and provide a "normal form" for spiral dynamics. In other words, one would hope that by making an appropriate expansion about the organizing center, one could reduce the infinite-dimensional reaction-diffusion problem to a low-dimensional system described by a few ordinary differential equations, that is, amplitude or normal-form equations [18, 38]. The resulting equations could then be analyzed to obtain a complete description of spiral meandering dynamics in the vicinity of the codimension-two point.

There is a problem, however, which makes this approach both difficult and interesting. The particular codimension-two bifurcation found for the spiral waves results from the interaction of Hopf and translational eigenmodes of a rotating wave, and existing bifurcation theory cannot be applied to such a case. The reason is that a theory has not been developed for noncompact symmetries such as translations. While translational symmetries are treated in many systems, this is done by requiring solutions to be spatially periodic and spiral waves are not (globally) periodic in space. Hence, it turns out that the codimension-two bifurcation at the heart of spiral meandering is of a fundamentally new type from the point of view of nonlinear dynamical systems.

While a rigorous derivation of a normal form will have to await advances in symmetric bifurcation theory, I will nevertheless proceed by proposing a low-dimensional model which contains the same codimension-two bifurcation as was observed in the reaction-diffusion equations, and I will show that this model contains the essence of spiral meandering.

5.1 Model equations

The model considered is the simplest system of ODEs which (*i*) has the symmetries important for the spiral dynamics (rotations, reflections, and translations), and which (*ii*) has a supercritical Hopf bifurcation from a rotating wave solution. The model equations are:

$$\begin{aligned} \dot{p} &= v, \\ \dot{v} &= v \cdot \left[f(|v|^2, w^2) + iw \cdot h(|v|^2, w^2) \right], \\ \dot{w} &= w \cdot g(|v|^2, w^2), \end{aligned} \tag{8}$$

where p and v are complex, and w is real. The real-valued functions f, g, and h are specified below. [Throughout this section, f and g will denote the above

functions in the ODE model equations and not the kinetics functions in Eqs. (2). There should be no confusion.] The model is of real dimension five because the codimension-two point being modeled has a five-dimensional center eigenspace. As the notation suggests, p is thought of as the position of the spiral tip and v its linear velocity. The instantaneous rotational frequency of solutions is proportional to w.

For any choice of f, g, and h, Eqs. (8) are invariant under the following transformations:

$$R_\gamma \cdot \begin{pmatrix} p \\ v \\ w \end{pmatrix} = \begin{pmatrix} e^{i\gamma} p \\ e^{i\gamma} v \\ w \end{pmatrix}, \qquad \kappa \cdot \begin{pmatrix} p \\ v \\ w \end{pmatrix} = \begin{pmatrix} p^* \\ v^* \\ -w \end{pmatrix},$$

$$T_{\alpha\beta} \cdot \begin{pmatrix} p \\ v \\ w \end{pmatrix} = \begin{pmatrix} p + \alpha + i\beta \\ v \\ w \end{pmatrix},$$

where $*$ denotes complex conjugation. R_γ is rotation by angle γ, κ is reflection, and $T_{\alpha\beta}$ is translation by $\alpha + i\beta$.

By letting the "position" be written $p = x + iy$ and the "velocity" be written $v = se^{i\phi}$, with "speed" $s \geq 0$, Eqs. (8) can be written in the alternative form:

$$\begin{aligned} \dot{x} = s\cos\phi, \qquad \dot{y} = s\sin\phi, \qquad \dot{\phi} = w \cdot h(s^2, w^2), \\ \dot{s} = s \cdot f(s^2, w^2), \qquad \dot{w} = w \cdot g(s^2, w^2). \end{aligned} \tag{9}$$

The simplest low-order expansions for f, g, and h sufficient to give the desired codimension-two bifurcation, and which yield bounded trajectories for the model, are:

$$\begin{aligned} f(s^2, w^2) &= -1/4 + \alpha_1 s^2 + \alpha_2 w^2 - s^4, \\ g(s^2, w^2) &= s^2 - w^2 - 1, \\ h(s^2, w^2) &= \gamma_0. \end{aligned} \tag{10}$$

Equations (8) and (10), or equivalently Eqs. (9) and (10), are then the proposed ODE model for spiral dynamics.

5.2 ODE MODEL DYNAMICS

Figure 10 shows a phase diagram for the ODE model as a function of the two parameters α_1 and α_2 with fixed γ_0. The diagram is plotted so as to emphasize its similarity to the spiral flower garden in Fig. 2. In the ODE model there exists a codimension-two point whose vicinity contains rotating waves, modulated rotating waves of both types (inward and outward petals), and modulated traveling waves. There is also a region in parameter space in which there are no such rotating solutions.

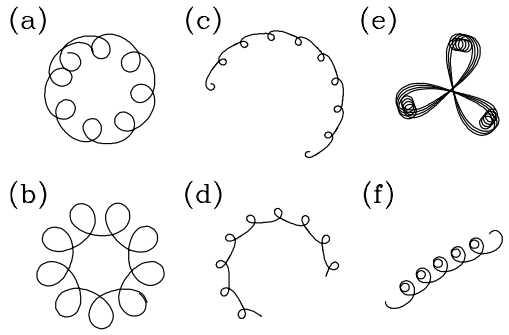

Fig. 10. Phase diagram for the ODE model with $\gamma_0 = 5.6$. There are three main regions: a region in which there are no rotating or modulated rotating solutions (hatched but not labeled), a region of stable periodic rotating-wave solutions, and a region of modulated-rotating-wave solutions. Shown are "tip-path" plots (x, y) at several parameter values. The periodic states are centered on the corresponding parameter points. The modulated rotating waves are of two types: those with inward petals and those with outward petals. Separating the two is a locus (dashed curve) of modulated traveling waves.

Figure 11 shows "tip-path" plots, (x, y), from the ODE model for several choices of α_1, α_2, and γ_0. Figs. 11(a)- 11(d) are examples which bear a striking resemblance to spiral tip paths in excitable media (cf. Fig. 1) and Refs. By choosing the three parameters appropriately, it is possible to reproduce essentially all types of spiral tip paths reported in the literature on homogeneous excitable media [7, 8, 9, 10, 11, 13, 15, 19]). It is also possible, however, to generate plots that do not correspond to any known spiral paths. Figures 11(e) and 11(f) show two such cases. These are cases for which the primary rotation frequency is large compared to the secondary rotation frequency. The choice of γ_0 is very important in determining the (x, y) flower patterns as well as the location of the MTW locus (dashed curve) in the phase diagram in Fig. 10. The remainder of this section is devoted to details of the ODE system.

5.3 Analysis of the model

The analysis of the ODE model begins by noting that the (s, w) subsystem in Eqs. (9) decouples from the other three equations and that $\phi(t)$, $x(t)$, and $y(t)$ can be found by quadrature once the last two equations are solved. Thus for much of the analysis to follow, one need only consider the dynamics of the (s, w) subsystem. For this it is useful to define variables ξ and ζ by: $\xi = s^2$ and $\zeta = w^2$. This yields the two-variable system:

$$\dot{\xi} = 2\xi f(\xi, \zeta) \qquad \dot{\zeta} = 2\zeta g(\xi, \zeta). \tag{11}$$

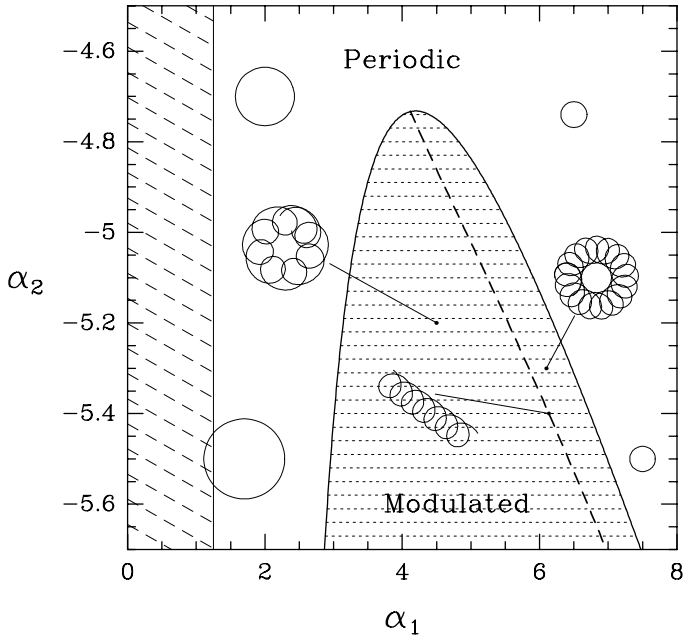

Fig. 11. Flowers obtain from the ODE model. Shown are plots of (x, y) for several choice of model parameter values. (a)-(d) are plots which resemble tip-path plots for spiral waves. (e) and (f) are plots which do not resemble known tip-path plots. The parameter values for the states shown are: (a) $\alpha_1 = 3.33$, $\alpha_2 = -6.75$, $\gamma_0 = 5.3$, (b) $\alpha_1 = 3.33$, $\alpha_2 = -6.75$, $\gamma_0 = 4.1$, (c) $\alpha_1 = 6.95$, $\alpha_2 = -5.8$, $\gamma_0 = 3.6$, (d) $\alpha_1 = 6.95$, $\alpha_2 = -5.8$, $\gamma_0 = 3.1$, (e) $\alpha_1 = 6.95$, $\alpha_2 = -5.8$, $\gamma_0 = 5.6$, (f) $\alpha_1 = 5.0$, $\alpha_2 = -5.5$, $\gamma_0 = 8.0$,

with,

$$f(\xi,\zeta) = -\frac{1}{4} + \alpha_1\xi + \alpha_2\zeta - \xi^2 \qquad g(\xi,\zeta) = \xi - \zeta - 1. \tag{12}$$

I shall refer to these equations as the reduced system, and to Eqs. (8), or equivalently Eqs. (9), as the full system. Note that because $s \geq 0$, $s = \sqrt{\xi}$, but there is no sign restriction on w so $w = \pm\sqrt{\zeta}$. The positive and negative values of w are related by reflectional symmetry κ.

5.3.1 Trivial steady state

The state $\xi = \zeta = 0$ is a steady state of Eqs. (11) for all parameter values, and by the choice of the constant terms in expansions for f and g, it is linearly stable for all values of α_1 and α_2. For the full system (8) this state corresponds to: $v = w = 0$, $p = p_0 =$ constant. The trivial steady state coexists with the rotating wave and modulated wave solutions discussed next. Hence the it plays much the

same role in the ODE model as the homogeneous steady state plays in excitable media. That is, in the reaction-diffusion model, the homogeneous state ($u = v = 0$ everywhere in space), exists and is linearly stable for all parameter values in the phase diagram (Fig. 2). The trivial steady state in the ODE model has the same character.

5.3.2 Rotating waves

Rotating waves in the full system (9) correspond to steady states in the reduced system with positive ξ and ζ. Letting ξ_1 and ζ_1 be positive roots of the steady state equations, $f(\xi_1, \zeta_1) = 0$ and $g(\xi_1, \zeta_1) = 0$, we have:

$$\begin{aligned} \xi_1^2 - (\alpha_1 + \alpha_2)\xi_1 + \alpha_2 + \frac{1}{4} = 0. \\ \zeta_1 = \xi_1 - 1. \end{aligned} \tag{13}$$

Only the larger root of Eq. (13) gives a state with positive ξ_1 and ζ_1.

To see that steady states of the reduced system correspond to rotating waves in the full system, first note that by the definition of ζ, $w = \pm\sqrt{\zeta_1}$. The equation for $\dot{\phi}$ in Eqs. (9) then becomes: $\dot{\phi} = \pm\gamma_0\sqrt{\zeta_1} \equiv \omega_1$, where ω_1 is the constant rotation frequency. This can be integrated to give $\phi(t) = \omega_1 t + \phi_0$, where ϕ_0 is a constant of integration. With this, the equations for $\dot{x}$ and $\dot{y}$ in Eqs. (9) can be integrated to obtain:

$$x(t) = x_0 + R\sin(\omega_1 t + \phi_0) \qquad y(t) = y_0 - R\cos(\omega_1 t + \phi_0) \tag{14}$$

where x_0 and y_0 are constants of integration and $R \equiv \pm\gamma_0^{-1}\sqrt{\xi_1/\zeta_1}$. Solutions (14) are rotating waves with frequency ω_1 and radius $|R|$. These rotating wave solutions come in counter-rotating pairs: $\omega_1 = \pm\gamma_0\sqrt{\zeta_1}$. Those with $\omega_1 > 0$ rotate in the opposite sense from those with $\omega_1 < 0$, and the reflection operator, κ, takes each of these waves into the other.

The rotating waves exist for $\alpha_1 > 5/4$. It can be shown easily from Eqs. (13) that as α_1 approaches $5/4$ from above, $\zeta_1 \to 0$. Hence the rotational frequency, ω_1, goes to zero, and the radius, $|R|$, diverges to infinity as α_1 approaches $5/4$. This is the behavior observed for spiral waves near the boundary between the region of periodic spirals and the region without spirals. Note the increase in tip-path radius with decreasing a in Fig. 7. This boundary in the spiral-wave system is not well understood from the point of view of bifurcation theory, and so detailed comparisons with the ODE model cannot be made at this time.

5.3.3 Modulated waves

Modulated waves in the full system correspond to limit-cycle behavior for ξ and ζ in the reduced system and the bifurcation to modulated waves corresponds to a Hopf bifurcation from a steady state (ξ_1, ζ_1) to a limit cycle. An expression for the

locus of Hopf bifurcations is obtained as follows. The stability matrix for Eqs. (11) is:

$$2\begin{bmatrix} \xi f_\xi(\xi,\zeta) & \xi f_\zeta(\xi,\zeta) \\ \zeta g_\xi(\xi,\zeta) & \zeta g_\zeta(\xi,\zeta) \end{bmatrix} \tag{15}$$

where subscripts denote differentiation and for now we drop the subscripts on ξ and ζ.

A necessary condition for a Hopf bifurcation is that the trace of the stability matrix be zero:

$$\xi f_\xi(\xi,\zeta) + \zeta g_\zeta(\xi,\zeta) = 0.$$

This gives

$$2\xi^2 - \alpha_1\xi + \zeta = 0. \tag{16}$$

This condition, together with the expressions for the rotating waves, Eq. (13), defines the Hopf locus in parameter space. (The determinant of (15) is always of the correct sign.) After a little algebra one obtains the following expression for the Hopf locus:

$$\xi_H = \frac{1}{4}\{(\alpha_1 - 1) + \sqrt{\alpha_1^2 - 2\alpha_1 + 9}\}$$
$$\alpha_2 = \frac{3 - 2(\alpha_1+1)\xi_H}{4(\xi_H - 1)}.$$

The first equation gives ξ_H, the value of ξ at the Hopf bifurcation, in terms of α_1. The second then gives α_2 for the Hopf bifurcation in terms of ξ_H and α_1. This Hopf locus is plotted in Fig. 10 and is the boundary of the region of modulated waves.

The MTW locus emerges from the Hopf locus at the codimension-two point where the Hopf frequency equals the rotation frequency. This point is easily found. We define ω_2 to be the Hopf frequency, that is $\omega_2 = \sqrt{\text{Det}}$, where Det is the determinant of the stability matrix (15) at the bifurcation. Then:

$$\begin{aligned} \omega_2^2 &= 4\xi\zeta\,(f_1 g_2 - f_2 g_1) \\ &= 4\xi\zeta\,(2\xi - \alpha_1 - \alpha_2) \end{aligned}$$

this can be simplified using Eq. (16) to give:

$$\omega_2^2 = 4\zeta\,(1 - (\alpha_2+1)\xi_H)$$

Thus the frequency ratio at any point along the Hopf locus is:

$$\left|\frac{\omega_2}{\omega_1}\right| = \frac{2}{\gamma_0}\sqrt{1 - (\alpha_2+1)\xi_H}$$

The codimension-two point is where $|\omega_2/\omega_1| = 1$ on the Hopf locus.

The frequency ratio $|\omega_2/\omega_1|$ depends on the parameter γ_0, in addition to the dependence on parameters α_1 and α_2, Hence the codimension-two point, and also the locus of MTW states which emerges from this point, depend on γ_0. The Hopf bifurcation locus in Fig. 10 is, however, independent of γ_0. Thus, by varying γ_0, it is possible to locate the codimension-two point anywhere on the Hopf curve, or to eliminate this point from the phase diagram entirely. The value chosen for γ_0 in Fig. 10 is such that the codimension-two point is at the apex of the Hopf curve, so that the phase diagram for the ODE model closely resembles the spiral phase diagram in Fig. 2. It is not understood at the present time why, for spiral waves in excitable media, the ratio between the primary and secondary frequencies is generally near one and why the codimension-two points often appear in the vicinity of a sharp turn in the Hopf locus.

Closed-form solutions are not known for the modulated waves which bifurcate from the rotating waves. Numerical integration of Eqs. (8) has been used to obtain the modulated waves shown in Figs. 10 and 11. The locus of MTW states (dashed curve in Fig. 10) has also been obtained numerically by searching for parameter values which give MTW states. From these simulations, it has been verified that the locus of Hopf bifurcations in Fig. 10 is everywhere supercritical, i.e. the various flower patterns grow continuously from circles.

6 Discussion and the future

Throughout this chapter I have taken the point of view that the meandering of spiral waves in excitable media can and should be examined from the perspective of bifurcation theory. With this approach, it has been possible to show that the organizing center for spiral dynamics is a particular codimension-two bifurcation resulting from the interaction of a Hopf bifurcation from rotating waves with symmetries of the plane. From this observation has followed a simple ordinary-differential-equation model for spiral meandering.

This work provides the first steps towards explaining why the spiral-tip flower patterns shown in Figs. 1 and 2 are so pervasive in experiments on, and simulations of, excitable media. From the bifurcation-theoretic view point such flowers follow inevitably when, in the presence of symmetries of the plane, a rotating wave becomes unstable at a frequency near its rotational frequency. This is true independently of system details. All the flowers seen in Figs. 10 and 11 are obtained from differential equations which do not depend on the properties of any particular excitable medium, and in a sense, apply universally to all excitable media.

There remains, then, a crucial open question "Why do periodically rotating spiral waves in excitable media become unstable in the first place ?" The analysis of the preceding section explains which dynamics can be expected *should* a spiral become unstable, but the analysis does not tell us why spirals become unstable or why the bifurcating frequency is generally close to the rotation frequency of the spiral wave. The answer to these questions depends, at least to some extent,

on the details of excitable media, and so must come from outside the bifurcation approach taken here. In this regard it is hoped that ongoing work on spiral waves using either the kinematical approach, e.g. Refs. [22, 40, 39], or the free-boundary approach, e.g. Refs. [41, 42, 43, 44, 45], will provide needed insight into the existence of the spiral organizing center.

Finally, even within the bifurcation approach, the ODE model presented is not complete. For example, including more variables in the model can affect its dynamics, as can higher-order terms in the functions f, g, and h in Eqs. (10). (These effects have not yet been considered because, as a first step, I wanted to consider only the simplest case.) Moreover, no direct correspondence has been established between parameters of the ODE model and the parameters of any excitable media, though a comparison of the phase diagrams for the ODE model and the reaction-diffusion equations suggests that this might be accomplished. There is every reason to believe that it will be possible to capture *completely* the dynamics of spiral waves in excitable media with a low-dimensional model similar to the ODE model considered in this chapter, in spirit if not in form.

References

1. B. P. Belousov, Sbornik Referatov po Radiacioni Medicine, p. 145 (1959).
2. A. Zaikin and A. M. Zhabotinskii, Nature **225**, 535 (1970).
3. A. T. Winfree, Science **181**, 937 (1973).
4. A. T. Winfree, *When Time Breaks Down* (Princeton Univ. Press, Princeton, 1987).
5. S. C. Müller, T. Plesser, and B. Hess, Science **230**, 661 (1985).
6. K. I. Agladze, A. V. Panfilov, A. N. Rudenko, Physica **29D**, 409 (1988).
7. W. Jahnke, W. E. Skaggs, and A. T. Winfree, J. Phys. Chem. **93**, 740 (1989).
8. T. Plesser, S. C. Müller, and B. Hess, J. Phys. Chem. **94**, 7501 (1990).
9. G. S. Skinner and H. L. Swinney, Physica **48D**, 1 (1991).
10. Z. Nagy-Ungvarai, J. Ungvarai, and S. C. Müller, Chaos **3**, 15 (1993).
11. V. S. Zykov, Biofizika **31**, 862 (1986).
12. E. Lugosi, Physica **40D**, 331 (1989).
13. D. Barkley, M. Kness, and L. S. Tuckerman, Phys. Rev. A **42**, 2489 (1990).
14. A. Karma, Phys. Rev. Lett. **65**, 2824 (1990).
15. A. T. Winfree, Chaos **1**, 303 (1991).
16. D. Barkley, Phys. Rev. Lett. **68**, 2090 (1992).
17. D. Barkley, "Euclidean symmetry and the dynamics of rotating spiral waves," preprint (1993).
18. J. Guckenheimer and P. Holmes, *Nonlinear Oscillations, Dynamical Systems, and Bifurcations of Vector Fields* (Springer, New York, 1983).
19. D. Barkley, Physica **49D**, 61 (1991).
20. V. S. Zykov, *Modelling of Wave Processes in Excitable Media* (Manchester Univ. Press, Manchester, 1988).
21. J. J. Tyson and J. P. Keener, Physica **32D**, 327 (1988).
22. A. S. Mikhailov and V. S. Zykov, Physica **52D**, 379 (1991).
23. E. Meron, Phys. Reports, **218**, 1 (1992).
24. V. I. Krinsky, Biophysics **11**, 776 (1966).
25. J. M. Greenberg and S. P Hastings, SIAM J. Appl. Math **34**, 515 (1978).
26. M. Gerhardt, H. Schuster, and J. J. Tyson, Science **247**, 1563 (1990).
27. M. Markus and B. Hess, Nature **347**, 56 (1990).
28. M. Kubíček and M. Marek, *Computational Methods in Bifurcation Theory and Dissipative*

Structures (Springer, New York, 1983).
29. Rüdiger Seydel, *From Equilibrium to Chaos: Practical Bifurcation and Stability Analysis* (Elsevier, New York, 1988).
30. Y. Saad and M. H. Schultz, SIAM J. Sci. Stat. Comp. **7**, 856 (1986).
31. I. Goldhirsch, S. A. Orszag, and B. K. Maulik, J. Sci. Comp. **2**, 33 (1987).
32. Y. Saad, *Numerical Methods for Large Eigenvalue Problems: Theory and Algorithms*, (John Wiley, New Yorrk, 1992).
33. D. S. Watkins, SIAM Review **35**, 430 (1993).
34. W. S. Edwards, L. S. Tuckerman, R. A. Friesner, and D. Sorensen, J. of Comp. Phys., (1994).
35. D. Ruelle, Arch. Rat. Mech. Anal. **51**, 136 (1973).
36. D. A. Rand, Arch. Rat. Mech. Anal. **79**, 1 (1982).
37. M. Kness, L. S. Tuckerman, and D. Barkley, Phys. Rev. A, **46**, 5054 (1992).
38. M. Golubitsky, I. Stewart, and D. G. Schaeffer, *Singularities and Groups in Bifurcation Theory, Vol. II* (Springer, New York, 1988).
39. E. Meron, Physica **49D**, 98 (1991).
40. P. Pelcé and J. Sun, Physica **48D**, 353 (1991).
41. J. P. Keener and J. J. Tyson, Physica **21D**, 307 (1986).
42. A. J. Bernoff, Physica **53D**, 125 (1991).
43. A. Karma, Phys. Rev. Lett. **68**, 397 (1992).
44. D. A. Kessler, H. Levine, and W. N. Reynolds, Phys. Rev. Lett. **68**, 401 (1992).
45. J. P. Keener, SIAM J. Appl. Math. **52**, 1370 (1992).